J. Plasma Phys. (2015), *vol.* 81, 905810502 © Cambridge University Press 2015
doi:10.1017/S0022377815000550

Image processing of argon glow discharge plasma using interferometry

A. M. Hamed[1,†] **and M. A. Saudy**[1]

[1]Physics Department, Faculty of Science, Ain Shams University, 11566 Cairo, Egypt

(Received 30 March 2015; revised 4 May 2015; accepted 5 May 2015)

In this paper, a method of processing argon plasma images, obtained from the DC pseudo glow discharge technique, using two- and multiple-beam interference is suggested. This method is based on measuring the image fringe shift from the background interference fringes. Hence, this mapping of intensity shift is related to the electron density distribution of the argon plasma. Also, the refractive index of the plasma is computed from the electron density values. The contrast of the interferometer images in presence of plasma shift is investigated in both cases of two- and multiple-beam interference.

1. Introduction

Many articles have developed interferometers that can be used to measure plasma parameters such as electron density and the nonlinear optical response in argon (Ar) and nitrogen (N_2) near the ionization threshold (Hug *et al.* 1967; Da Silva, Barbee & Cauble 1995; Osten *et al.* 2001; Scime *et al.* 2001; Keyser *et al.* 2003; Wahlstrand *et al.* 2011). The refractive index of argon plasma was measured early in Hug *et al.* (1967) using a Mach–Zehnder interferometer. A technique based on a swept microwave interferometer was used to optimize the electron density measurements in a steady-state problem (Scime *et al.* 2001).

Plasma is normally composed of molecules, ions, and free electrons. The refractive index of plasma is not only determined by atoms or molecules like common gases, but also by the electrons and ions. The relation between the dispersion and the temperature of argon plasma is deduced from the plasma refractive index equation (Yun *et al.* 2008). The digital image processing technique is considered as a low-cost and non-invasive probing technique to measure different physical parameters like energy, temperature, and density of glow discharge plasma (Kodal, Majumder & Deka 2011).

Holographic interferometry can also be applied to plasma whose density results in shifts of less than one fringe by superposing the small shifts on an arbitrarily shaped and positioned background fringe pattern. The sensitivity of holographic interferometry is thereby increased to that of conventional interferometry, while the inherent advantages of holography are retained. The background fringes also simplify detection of the spurious phase changes that can arise in holography from motions of the apparatus (Jahoda, Jeffries & Sawyer 1967). Image processing of argon plasma

† Email address for correspondence: amhamed73@hotmail.com

https://doi.org/10.1017/S0022377815000550 Published online by Cambridge University Press

using Fourier holography has been investigated. The decoded images were improved using Wiener filtering (Hamed & Saudy 2014).

A recent technique based on pump–probe interferometry allows investigations of ultra-fast dynamics of laser plasma and gives high-resolution interferometry images (Garnov *et al.* 2003).

Quantitative evaluation of interference fields for the interferometry measurements consists of the pointwise determination of the phase difference $\Delta\phi$ between the reference beam and the object beam that interfere. Phase values are closely related to the optical path difference between these two beams. The physical quantity to be measured, e.g. displacement, can then be determined from the phase distribution (Yatagai & Nakadate 1982; Robinson & Reid 1993; Kreis 1996; Mikš & Novak 2001).

In this study, the interferometry method is based on introducing the plasma image inside the central region of the interference pattern. The computation of the fringe shift is originated due to presence of the plasma image using two-beam interference. Secondly, we use multiple-beam interference, which improves the image contrast. Thirdly, the image contour and the autocorrelation images are obtained at different phases. We deduce the electron density of the plasma and the corresponding refractive index from the intensity fringe shift. Finally, results and discussions are presented followed by a conclusion.

2. Theoretical analysis

The assumed distribution of the intensity of the two-beam interference in the detector plane can be expressed as follows:

$$I_1(x, y) = a(x, y) + b(x, y)\cos[\Delta\Phi'(X, Y)], \tag{2.1}$$

where $I_1(x, y)$ is the intensity of the interference field in the point (x, y), $a(x, y)$ is the function that characterizes the mean intensity of the interference pattern, and $b(x, y)$ is the function that determines the modulation of the interference signal.

This work focuses on the main technique for phase evaluation of the argon plasma image using the phase-shifting method. Hence, adding the phase information of the image $\psi(x, y)$ in (2.1), we can write it as follows:

$$I_2(x, y) = a(x, y) + b(x, y)\cos[\Delta\Phi'(x, y) - \Psi(x, y)]. \tag{2.2}$$

In order to improve the image contrast of the phase object, multiple-beam interference can be used. In this case, the transmitted intensity distribution is mathematically represented by the known expression of the Airy distribution (Tolansky 1960; Barakat & Mokhtar 1963; Barakat 1971; Hamed 1976, 2008) as follows:

$$I(r') = \frac{1}{(1 - r^2) + 4r^2\sin^2[\Delta\Phi'(x, y) - \Psi(x, y)]}, \tag{2.3}$$

where $r'(x', y')$ is the imaging plane and r is the amplitude reflection coefficient of either of the interferometer plates.

The axial image shift is computed from the following formula (Hamed 1976):

$$L_a = (\delta z/\Delta Z)\cdot\lambda/2, \tag{2.4}$$

https://doi.org/10.1017/S0022377815000550 Published online by Cambridge University Press

where δz is the fringe shift of the plasma image and ΔZ is the inter-fringe spacing, which equals $\lambda/2$.

The critical density of the plasma (n_c) is defined by the following equation:

$$\omega = \left(\frac{n_c e^2}{m_e \varepsilon_0}\right)^{1/2} \rightarrow n_c = \frac{m_e \varepsilon_0}{e^2}\omega^2, \tag{2.5}$$

$$\omega \text{ (wave)} = \omega_p \text{ (plasma)}. \tag{2.6}$$

Hence, the critical density becomes

$$n_c = \frac{4\pi^2 c^2 m_e \varepsilon_0}{\lambda^2 e^2} = \frac{1.1148 \times 10^{15} \text{ m}^{-1}}{\lambda^2 \text{ [m]}^2}. \tag{2.7}$$

Consequently, the plasma refractive index can be written as follows:

$$N = \left(1 - \frac{n_e}{n_c}\right)^{1/2} \rightarrow N = 1 - \frac{1}{2}\frac{n_e}{n_c}, \tag{2.8}$$

where $\omega \gg \omega_p \rightarrow n_e \ll n_c$ represents the condition of propagation.

The phase of the wave accumulated by travelling a distance L in a medium is

$$\Phi(x, y) = \int_L k \, \mathrm{d}l = \int \frac{N\omega}{c} \, \mathrm{d}l. \tag{2.9}$$

Then the same wave that propagates over two equivalent paths L in plasma and in vacuum gives the phase difference as follows:

$$\Delta\Phi(x, y) = \int (k - k_0) \, \mathrm{d}l = \int (N - 1)\frac{\omega}{c} \, \mathrm{d}l. \tag{2.10}$$

Substituting from (2.8) in (2.10), we get

$$\Delta\Phi(x, y) = \frac{\omega}{2cn_c} \int n_e(x, y, z) \, \mathrm{d}z, \quad \omega = 2\pi c/\lambda. \tag{2.11}$$

Hence, the phase density of the plasma is proportional to the line integral of the electron density and inversely proportional to the wavelength λ.

2.1. *Computation of the argon plasma phase from the two-beam interference pattern*

The phase information of the argon plasma can be extracted in two-beam interference as follows:

(i) Introduce the phase $\pi/2$ in (2.2), the we write the intensity distribution as:

$$I_3(x, y) = a(x, y) + b(x, y) \cos[\Delta\Phi'(x, y) - \Psi(x, y) - \pi/2]. \tag{2.12}$$

(ii) Introduce the phase $3\pi/2$; then we write the intensity distribution as

$$I_4(x, y) = a(x, y) + b(x, y) \cos[\Delta\Phi'(x, y) - \Psi(x, y) - 3\pi/2]. \tag{2.13}$$

https://doi.org/10.1017/S0022377815000550 Published online by Cambridge University Press

(iii) Introduce the phase $5\pi/2$; then we write the intensity distribution as

$$I_5(x, y) = a(x, y) + b(x, y)\cos[\Delta\Phi'(x, y) - \Psi(x, y) - 5\pi/2]. \tag{2.14}$$

From (2.12) and (2.14), we obtain the phase information of the plasma image as follows:

$$\Delta\Phi'(x, y) - \Psi(x, y) = \tan^{-1}\left[\frac{I_5(x, y) - I_4(x, y)}{I_3(x, y) - I_4(x, y)}\right]. \tag{2.15}$$

The distance between any two fringes $= \lambda/2$. Consequently, the phase information of the plasma image is governed by the following equation:

$$\Psi(x, y) = \Delta\Phi'(x, y) - \tan^{-1}\left[\frac{I_5(x, y) - I_4(x, y)}{I_3(x, y) - I_4(x, y)}\right], \tag{2.16}$$

where the range of the interference phase $\Phi'(x, y)$ extends from 0 up to 2π.

In this case, making use of the phase difference governed by (2.11) and substituting in (2.15), we get

$$\tan^{-1}\left[\frac{I_5(x, y) - I_4(x, y)}{I_3(x, y) - I_4(x, y)}\right] = \frac{\omega}{2cn_c}\int n_e(x, y, z)\,\mathrm{d}z = \frac{\omega}{2cn_c}n_e(x, y)L. \tag{2.17}$$

In (2.17), we have put $\Delta\Phi(x, y) = \Delta\Phi'(x, y) - \Psi(x, y)$. It represents the difference between the phase in presence of plasma and the phase in absence of plasma (background fringes), respectively, and L is the plasma axial length. Hence, we can get the plasma electron density from (2.17).

From (2.8) and (2.17), we get the refractive index distribution of the argon plasma as follows:

$$N(x, y) = 1 - \frac{\lambda}{2\pi L}\left\{\tan^{-1}\left[\frac{I_5(x, y) - I_4(x, y)}{I_3(x, y) - I_4(x, y)}\right]\right\}. \tag{2.18}$$

This equation is rewritten as a function of the plasma image phase as follows:

$$N(x, y) = 1 - \left(\frac{\lambda}{2\pi L}\right)\Psi(x, y). \tag{2.19}$$

Equations (2.18) and (2.19) show that the plasma refractive index depends on the plasma image intensities in the interval $[0, 2\pi]$ or the plasma phase and the plasma wavelength λ. Also, the plasma refractive index (N) has a nearly linear distribution with the plasma electron density given by (2.8).

2.2. *Computation of the plasma refractive index from the image fringe shift*

The obtained plasma fringe images shown in figure 3 are represented in the y–z plane. Hence, from (2.10), the shift along the axial z direction is represented as follows:

$$\Delta\Phi(y; z) = \left(\frac{2\pi}{\lambda}\right)[N(y; z) - 1]L. \tag{2.20}$$

The plasma refractive index is computed directly from the phase image shift as follows:

$$N(y; z) = 1 + \left(\frac{\lambda}{2\pi L}\right)\Delta\Phi(y; z). \tag{2.21}$$

https://doi.org/10.1017/S0022377815000550 Published online by Cambridge University Press

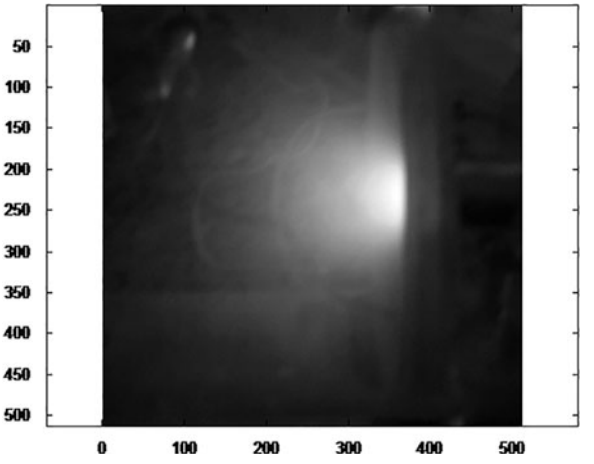


FIGURE 1. Argon plasma image used in the processing. It has dimensions of 512 pixels × 512 pixels.

Also, the plasma electron density is computed from the fringe shift using (2.17) as

$$n_e(y;\, z) = n_c \left(\frac{\lambda}{\pi L}\right) |\Delta\Phi(y;\, z)|. \tag{2.22}$$

The phase of the image is represented as follows:

$$\Delta\Phi(y;\, z) = 2\pi \left(\frac{\delta z}{\Delta z}\right), \tag{2.23}$$

where δz is the fringe shift with respect to fringe spacing Δz.

Since $\Delta\Phi(y;\, z)$ has a shift directed towards the cathode, it has a negative value. Consequently, (2.21) can be rewritten in terms of the fringe shift as follows:

$$N(y;\, z) = 1 - \left(\frac{\lambda}{L}\right)\left(\frac{\delta z}{\Delta z}\right). \tag{2.24}$$

The results of n_e and N represented by the plots shown in figure 10 and tables 2–6 are computed using (2.22) and (2.24). In the above computations, we have taken the wavelength as $\lambda = 600$ nm and $L = 10\pi = 60$ mm, the diameter of the phase image to represent the plasma length along the z axis. The inter-fringe spacing $\Delta z = 34$ pixels. The refractive index of the plasma is always less than 1.

3. Results and discussion

The argon plasma image photographed in the laboratory by a CCD camera is obtained using the DC glow discharge technique (Saudy 2009). The argon plasma image used in the processing is shown in figure 1. It has dimensions of 512 pixels × 512 pixels. The contour image of the argon plasma is plotted in figure 2. The interference shift of the argon plasma image using two-beam interference is obtained as shown in figure 3. Five horizontal discontinuous lines at 130, 180, 230, 280, and 330 pixels are represented in the same figure in order to compute the plasma fringe shifts.

https://doi.org/10.1017/S0022377815000550 Published online by Cambridge University Press

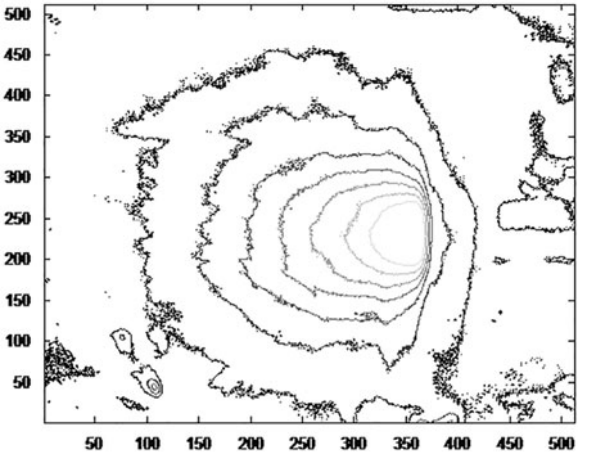


FIGURE 2. Contour of the plasma image in the whole image of dimensions 512 pixels × 512 pixels.

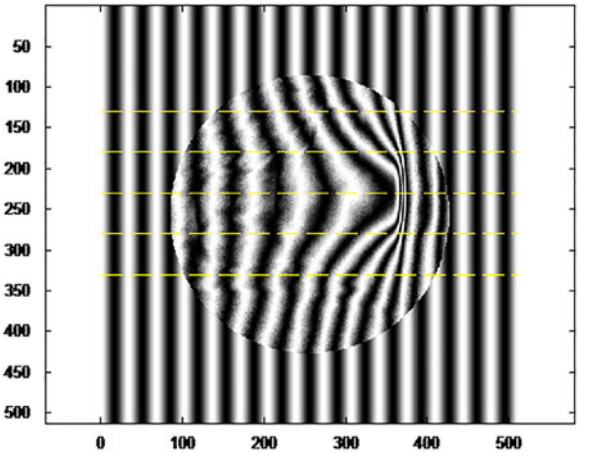


FIGURE 3. Interferometry shift of argon plasma image using two-beam interference. The image has dimensions of 512 pixels × 512 pixels, and the shifted image is located in a circle of diameter equal to $10\pi = (512 \times 6/8.6)$ as compared with the total image of $15\pi = 512$ pixel. Five horizontal discontinuous lines are shown at 130, 180, 230, 280, and 330 pixels to compute plasma fringe shifts represented in figure 10.

The shifted central image is located inside a circle of diameter equal to $10\pi = (512 \times 6/8.6)$ as compared with the total image of $15\pi = 512$ pixels. The phase image of argon plasma is computed from (2.10) using Matlab code. It is shown in figure 4. All images in figures 1–4 have dimensions of 512 pixels × 512 pixels.

Two profiles at horizontal section, at 230 pixel, one for the uniform two-beam interference while the second is for the plasma-shifted interference, are plotted in figure 5.

Equation (2.3), which describes the intensity distribution of the multiple-beam interference, is used to draw the intensity map of the argon plasma superimposed over the interference pattern. Images at different frequencies of the interference

https://doi.org/10.1017/S0022377815000550 Published online by Cambridge University Press

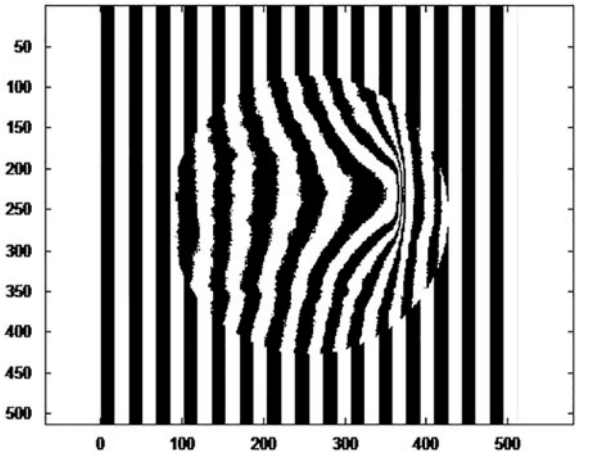


FIGURE 4. The phase image of argon plasma calculated directly using the arc tan function (2.10).

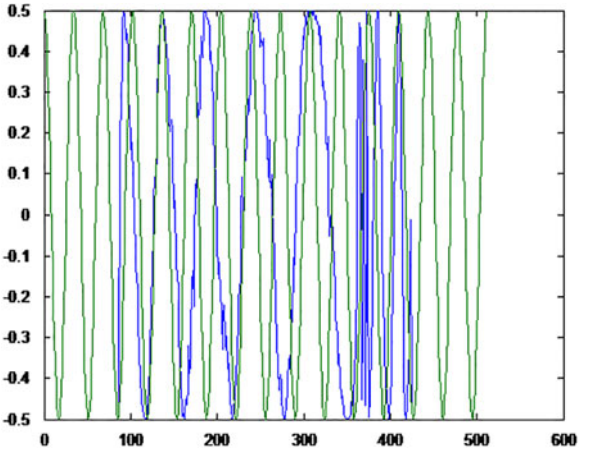


FIGURE 5. Two profiles taken at horizontal section at 230 pixel, one for the uniform two-beam interference while the second is for the plasma-shifted interference.

pattern are plotted in figure 6(*a–d*). In case of multiple-beam interference a sharper fringe shift is obtained as compared with two-beam interference. This is useful to get an accurate measurement of the fringe shift in case of multiple-beam interference as compared with the two-beam interference fringe shift.

Two profiles at horizontal section 230 pixel, one for the background multiple-beam fringe system while the second is for the plasma-shifted interference, are plotted in figure 7.

The autocorrelation of the argon plasma image of dimensions 512 pixels $\times$ 512 pixels is shown in figure 8. The profiles of the autocorrelation of the argon image at different horizontal sections is shown in figure 9. Eight plots are shown from the highest at 256 pixel followed by 200, 170, 150, 130, 100, 80, and 50 pixels.

The relation between the distance along the z axis in mm and the axial shift of the image in nm is computed from (2.4), using table 1. As shown in figure 9, the highest

https://doi.org/10.1017/S0022377815000550 Published online by Cambridge University Press

Dist. in pixel	Interference order (n)	δz mm at 180 pixel	δz mm at 230 pixel	δz mm at 280 pixel	L in nm at 180 pixel	L in nm at 230 pixel	L in nm at 280 pixel
12	1	0	0	0	0	0	0
24	2	0	0	0	0	0	0
36	3	0	−4	−3	0	−100	−75
48	4	1	0	0	25	0	0
60	5	5	5	4	125	125	100
72	6	11	14	10	275	350	250
84	7	12	24	18	300	600	450
96	8	21	30	21	525	750	525
108	9	19	22	19	475	550	475
120	10	10	11	11	250	275	275
132	11	2	4	2	50	100	50
144	12	0	0	−1	0	0	−25
156	13	0	0	0	0	0	0
168	14	0	0	0	0	0	0

TABLE 1. The axial shift occurring in the fringe system of two-beam interference, where the wavelength of illumination of the interferometer is $\lambda = 600$ nm, and the distance between two successive fringes $\Delta z = 12$ mm in the image of total dimensions 512 pixels × 512 pixels corresponding to dimensions of 11.5 cm × 17.2 cm at magnification of $M = 1.8$. Fourteen fringes are shown as in figure 6(*c*).

Z axial (mm)	δz (pixel)	$\left(\frac{\delta z}{\Delta z}\right)$	$\lvert\Delta\Phi(y;z)\rvert$	$n_e(y;z)$ (m^{-3})	$[1-N(y;z)]\times 10^{-6}$
6	0	0	0	0	0
12	0	0	0	0	0
18	0	0	0	0	0
24	0	0	0	0	0
30	0	0	0	0	0
36	10	0.294	1.847	18.23×10^{21}	2.94
42	15	0.441	2.771	27.35×10^{21}	4.41
48	18	0.529	3.324	32×10^{21}	5.29
54	21	0.618	3.883	38.33×10^{21}	6.18
60	12	0.353	2.218	21.89×10^{21}	3.53
66	0	0	0	0	0
72	0	0	0	0	0
78	0	0	0	0	0
84	0	0	0	0	0

TABLE 2. Computed values of the plasma phase shift $\Delta\phi(y;z)$, the plasma electron density $n_e(y;z)$, and its refractive index $N(y;z)$ from the fringe shift at 130 pixel.

fringe shift is located at the horizontal line at 230 pixel while the other two fringe shifts are located at horizontal lines 180 and 280 pixels. In the figure, the continuous line is drawn at 180 pixel while the discontinuous line is at 280 pixel.

https://doi.org/10.1017/S0022377815000550 Published online by Cambridge University Press

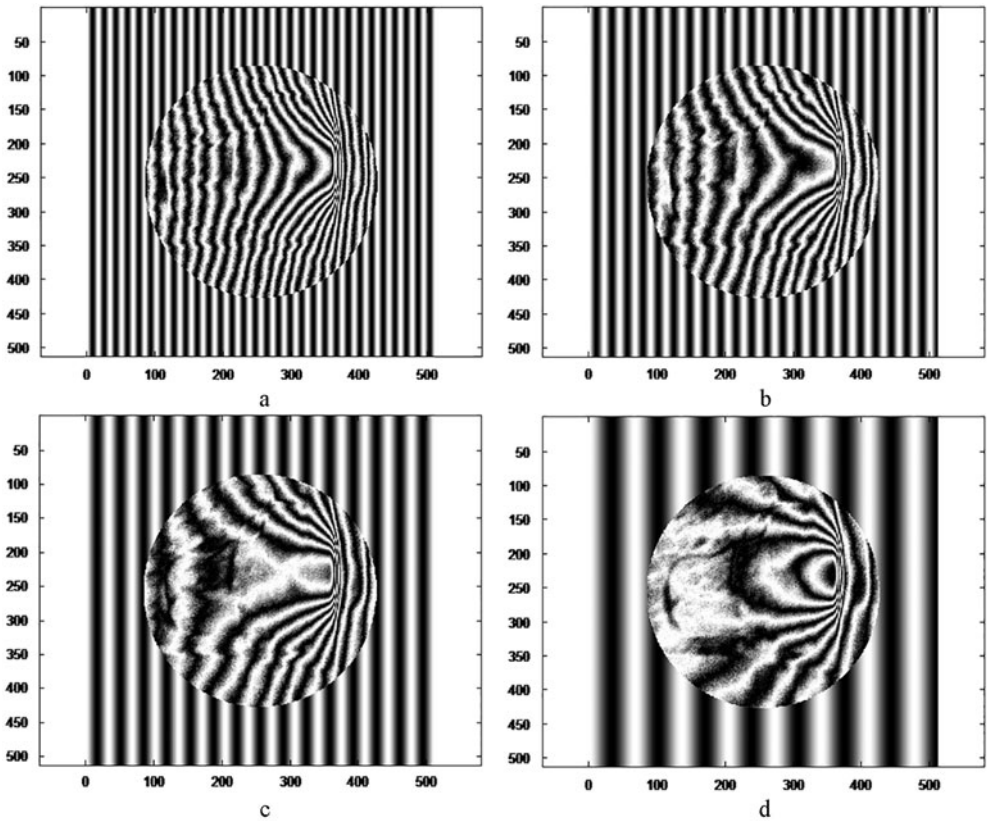


FIGURE 6. (*a*) Multiple-beam interference, where $F(x, y) = \sin^2(2 * y - \psi(x, y))$. Twenty-nine fringes are shown as background fringes. (*b*) Multiple-beam interference, where $F(x, y) = \sin^2(3 * y/2 - \psi(x, y))$. Twenty-two fringes are shown as background fringes. (*c*) Multiple-beam interference, where $F(x, y) = \sin^2(y - \psi(x, y))$. Fourteen fringes are shown as background fringes. (*d*) Multiple-beam interference, where $F = \sin^2(y/2 - \psi(x, y))$. Seven fringes are shown as background fringes.

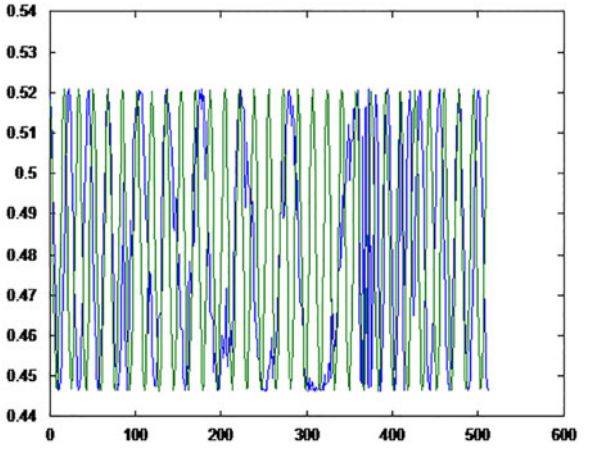


FIGURE 7. Two profiles taken at horizontal section at 230 pixel, one for the uniform multiple-beam interference while the second is for the plasma-shifted interference.

https://doi.org/10.1017/S0022377815000550 Published online by Cambridge University Press

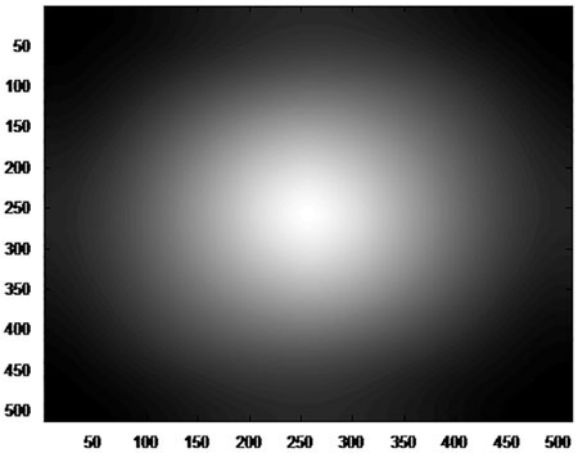


FIGURE 8. Autocorrelation of the argon plasma image of dimensions 512 pixels × 512 pixels.

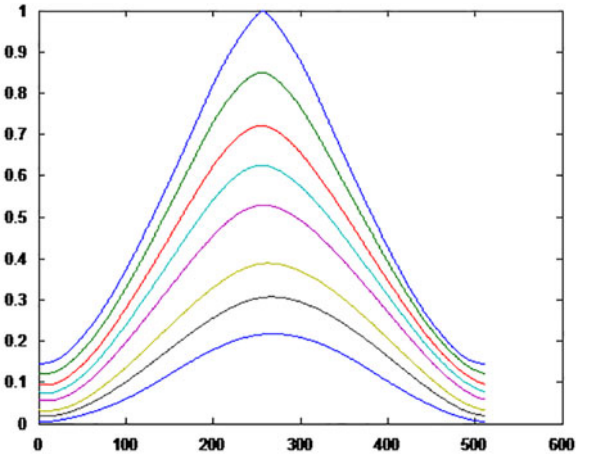


FIGURE 9. Profiles of the autocorrelation of the argon image at horizontal sections. Eight plots are shown from the highest at 256 pixel followed by 200, 170, 150, 130, 100, 80, and 50 pixel.

The relation between the distance along the z axis in pixels and the axial shift of the image in nm computed from (2.4) using two-beam interference is shown in figure 10. Five curves are plotted where the highest fringe shift is located at the line 230 pixel. Two other plots show a moderate shift for the red and blue curves at 180 and 280 pixels. The lowest two curves for shift are for 130 and 330 pixels. From the curves it is shown that the highest fringe shift is located near the plasma electrodes for the line 230 pixel while on moving farther from the electrodes the fringe shift decreases in proportion to its intensity. Hence, a plasma fringe mapping is obtained from the above results.

https://doi.org/10.1017/S0022377815000550 Published online by Cambridge University Press

Z axial (mm)	δz (pixel)	$\left(\frac{\delta z}{\Delta z}\right)$	$\lvert\Delta\Phi(y;z)\rvert$	$n_e(y;z)$ (m^{-3})	$[1-N(y;z)]\times 10^{-6}$
6	0	0	0	0	0
12	0	0	0	0	0
18	0	0	0	0	0
24	2	0.059	0.371	3.66×10^{21}	0.94
30	15	0.441	2.771	27.35×10^{21}	7.04
36	30	0.882	5.542	54.70×10^{21}	14.077
42	46	1.353	8.501	83.90×10^{21}	21.59
48	56	1.647	10.348	102.13×10^{21}	26.28
54	51	1.5	9.428	93.05×10^{21}	23.95
60	27	0.794	4.989	49.24×10^{21}	12.67
66	3	0.088	0.553	5.458×10^{21}	1.404
72	−1	−0.029	0.182	3.66×10^{21}	0.46
78	0	0	0	0	0
84	0	0	0	0	0

TABLE 3. Computed values of the plasma phase shift $\Delta\phi(y;z)$, the plasma electron density $n_e(y;z)$, and its refractive index $N(y;z)$ from the fringe shift at 180 pixel.

Z axial (mm)	δz (pixel)	$\left(\frac{\delta z}{\Delta z}\right)$	$\lvert\Delta\Phi(y;z)\rvert$	$n_e(y;z)$ (m^{-3})	$[1-N(y;z)]\times 10^{-6}$
6	0	0	0	0	0
12	0	0	0	0	0
18	−3	−0.09	0.56	5.53×10^{21}	−0.23
24	11	0.32	2.01	19.84×10^{21}	0.813
30	16	0.47	2.95	29.12×10^{21}	1.194
36	36	1.06	6.66	65.73×10^{21}	2.69
42	70	2.06	12.94	127.72×10^{21}	5.23
48	90	2.65	16.65	164.33×10^{21}	6.73
54	61	1.79	11.25	111.04×10^{21}	4.55
60	31	0.91	5.72	56.46×10^{21}	2.31
66	10	0.29	1.82	17.96×10^{21}	0.74
72	−3	−0.09	0.56	5.53×10^{21}	−0.23
78	0	0	0	0	0
84	0	0	0	0	0

TABLE 4. Computed values of the plasma phase shift $\Delta\phi(y;z)$, the plasma electron density $n_e(y;z)$, and its refractive index $N(y;z)$ from the fringe shift at 230 pixel.

4. Conclusion

We have extracted phase information of a plasma image using two-beam interference. A formula giving the phase shift of the image was derived. Also, a relation between the fringe shift and the plasma electron density was obtained. Consequently, the plasma refractive index was computed from the derived electron density. The

https://doi.org/10.1017/S0022377815000550 Published online by Cambridge University Press

Z axial (mm)	δz (pixel)	$\left(\frac{\delta z}{\Delta z}\right)$	$\lvert\Delta\Phi(y;z)\rvert$	$n_e(y;z)$ (m^{-3})	$[1-N(y;z)]\times 10^{-6}$
6	0	0	0	0	0
12	0	0	0	0	0
18	−7	0.205	1.29	12.73×10^{21}	0.52
24	3	0.09	0.56	5.53×10^{21}	0.23
30	12	0.35	2.2	21.71×10^{21}	0.89
36	27	0.79	4.96	48.95×10^{21}	2.01
42	46	1.35	8.48	83.70×10^{21}	3.43
48	55	1.62	10.18	100.48×10^{21}	4.11
54	56	1.65	10.37	102.35×10^{21}	4.19
60	32	0.94	5.91	58.33×10^{21}	2.39
66	2	0.06	0.38	9.82×10^{21}	0.15
72	−6	−0.176	1.11	10.96×10^{21}	0.45
78	0	0	0	0	0
84	0	0	0	0	0

TABLE 5. Computed values of the plasma phase shift $\Delta\phi(y;z)$, the plasma electron density $n_e(y;z)$, and its refractive index $N(y;z)$ from the fringe shift at 280 pixel.

Z axial (mm)	δz (pixel)	$\left(\frac{\delta z}{\Delta z}\right)$	$\lvert\Delta\Phi(y;z)\rvert$	$n_e(y;z)$ (m^{-3})	$[1-N(y;z)]\times 10^{-6}$
6	0	0	0	0	0
12	0	0	0	0	0
18	0	0	0	0	0
24	0	0	0	0	0
30	1	0.029	0.182	1.8×10^{21}	0.074
36	12	0.353	2.22	21.91×10^{21}	0.897
42	18	0.529	3.32	32.77×10^{21}	1.34
48	16	0.47	2.95	29.12×10^{21}	1.19
54	17	0.5	3.14	30.99×10^{21}	1.27
60	15	0.441	2.77	27.34×10^{21}	1.12
66	2	0.06	0.38	3.75×10^{21}	0.152
72	−12	−0.353	2.22	21.91×10^{21}	−0.9
78	0	0	0	0	0
84	0	0	0	0	0

TABLE 6. Computed values of the plasma phase shift $\Delta\phi(y;z)$, the plasma electron density $n_e(y;z)$, and its refractive index $N(y;z)$ from the fringe shift at 330 pixel.

multiple-beam interference images for the plasma shift showed higher contrast as compared with the images obtained in case of two-beam interference. Hence, accurate measurement of the fringe shift is attained.

https://doi.org/10.1017/S0022377815000550 Published online by Cambridge University Press

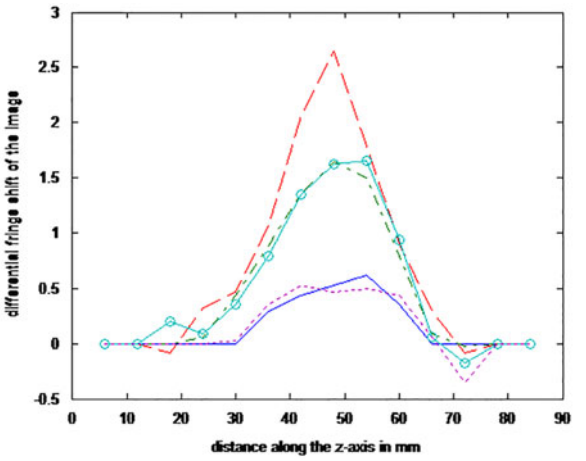


FIGURE 10. Five curves are plotted in the figure between the differential fringe shift $\delta z/\Delta z$ and the distance along the axial plasma length in mm. The highest fringe shift is located at 230 pixel for the red curve. Two plots show a moderate shift at 180 and 280 pixels. The lowest two curves for shift are for 130 and 330 pixels.

Finally, the autocorrelation image of the argon plasma image and the corresponding profiles at different sections were made. All interference images for plasma, the contour, and correlation images were fabricated using Matlab code.

REFERENCES

BARAKAT, N. 1971 Interferometric studies of fibers. *Textile Res. J.* **41**, 167.

BARAKAT, N. & MOKHTAR, S. 1963 On the factors contributing to the formation of multiple-beam Fizeau fringes. *J. Opt. Soc. Amer.* **53**, 300–301.

GARNOV, S. V., KONOV, V. I., MALYUTIN, A. A., TSARKOVA, O. G., YATSKOVSKY, S. & DAUSINGER, F. 2003 High resolution interferometric diagnostics of plasma produced by ultra-short laser pulses. *Laser Phys.* **13**, 386–396.

HAMED, A. M. 1976 Some applications of scattered light and multiple beam interference using coherent light, MSc thesis, Ain Shams University, Cairo, Egypt.

HAMED, A. M. 2008 Modeling of the fringe shift in multiple beam interference in glass for glass fibers. *Pramana J. Phys.* **70**, 643–648.

HAMED, A. M. & SAUDY, M. A. 2014 Holographic imaging of argon plasma images. *Opt. Photon. J.* **4**, 136–142.

HUG, W. F., EVANS, D., TANKIN, R. S. & CAMBEL, A. B. 1967 Measured index of refraction for argon plasma. *Phys. Rev.* **162**, 117.

JAHODA, F. C., JEFFRIES, R. A. & SAWYER, G. A. 1967 Fractional fringe holographic plasma interferometry. *Appl. Opt.* **6**, 1407–1410.

KEYSER, C., SCHRIEVER, G., RICHARDSON, M. & TURCU, E. 2003 Studies of high-repetition-rate laser plasma EUV sources from droplet targets. *Appl. Phys.* A **77**, 217–221.

KODAL, A., MAJUMDER, S. & DEKA, U. 2011 Measurement of plasma parameters using digital image processing technique. *Proc. Int. J. Comput. Appl.* 22–27.

KREIS, T. 1996 *Holographic Interferometry: Principles and Methods*. Akademie.

MIKŠ, A. & NOVAK, J. 2001 Application of multi-step algorithms for measurement deformation. In *SPIE Proceedings, Washington*, vol. 4398.

https://doi.org/10.1017/S0022377815000550 Published online by Cambridge University Press

OSTEN, W., BAUMBACH, T., SEEBACHER, S. & JUPTNER, W. 2001 Automatic processing of fringe pattern. In *Proceedings of 4th International Workshop on Automatic Processing of Fringe Patterns* (ed. W. Juptner & W. Osten), pp. 373–382. Akademie.

ROBINSON, D. W. & REID, G. T. 1993 *Interferogram Analysis: Digital Fringe Pattern Measurement Techniques*. Institute of Physics.

SAUDY, M. A. 2009 DC pseudo glow discharge in nitrogen gas. *Plasma Devices Oper.* **17**, 88–96.

SCIME, E. E., BOIVIN, R. F., KLINE, J. L. & BALKEY, M. M. 2001 Microwave interferometer of steady state plasma. *Rev. Sci. Instrum.* **72**, 1672–1676.

DA SILVA, L. B., BARBEE, T. W. JR, CAUBLE, R., CELLIERS, P., CIARLO, D., MORENO, J. C., MROWKA, S., TREBES, J. E., WAN, A. S. & WEBER, F. 1995 Development of XUV interferometry (155 Å) using a soft x-ray laser. In *SPIE 40th Annu. Meet., San Diego, CA, 9–14 July*.

TOLANSKY, S. 1960 *Surface Micro-Topography*. Longmans Green.

WAHLSTRAND, J. K., CHENG, Y. H., CHEN, Y. H. & MILCHBERG, H. M. 2011 Optical nonlinearity in Ar and N_2 near the ionization threshold. *Phys. Rev. Lett.* **107**, 1–5.

YATAGAI, T. & NAKADATE, S. 1982 Automatic fringe analysis using digital image processing technique. *Opt. Engng.* **21**, 432–435.

YUN, C. Y., YANG, S., ZHI, H. A. & HUA, L. Z. 2008 Dependence of arc plasma dispersion capability on its temperature. *Chinese Phys. Lett.* **25**, 4258–4261.

https://doi.org/10.1017/S0022377815000550 Published online by Cambridge University Press